

Avoiding Interpolation Errors for Computed Second Virial Coefficients of Noble Gases

Allan H. Harvey

Applied Chemicals and Materials Division, National Institute of Standards and Technology, Boulder, Colorado, 80305-3337, USA

E-mail: allan.harvey@nist.gov

Giovanni Garberoglio

European Centre for Theoretical Studies in Nuclear Physics and Related Areas (FBK-ECT*), Trento, I-38123, Italy

E-mail: garberoglio@ectstar.eu

20 August 2025

Abstract. Virial coefficients for noble gases calculated from first principles play a key role in gas-based temperature and pressure metrology. They have typically been presented in tabular form, but as smaller uncertainties are achieved the uncertainty introduced by interpolation between tabulated points can become significant. We demonstrate these interpolation errors for the second density and acoustic virial coefficients of ^4He and for the second density virial coefficients of Ne and Ar. We then offer an alternative approach, using simple scripts along with a data structure containing precalculated phase shifts to generate these coefficients at any temperature of metrological interest. The approach is applied to the state-of-the-art pair potentials for ^3He , ^4He , Ne, and Ar, and the software and data tables are made available for general use.

Keywords: argon; helium; interpolation; neon; phase shifts; second virial coefficients; uncertainty

Revision submitted to *Metrologia*.

1. Introduction

Thermodynamic metrology for temperature and pressure increasingly utilizes the ability to make very accurate acoustic [1, 2], dielectric [3, 4, 5], or refractive [6, 7, 8, 9, 10, 11, 12] measurements of gases. These gas-phase measurements in turn take advantage of the ability to calculate from first principles properties of noble gases, especially helium, with uncertainties much smaller than those attainable by experiment [13].

In this work, our concern is the virial coefficients that enable rigorous calculation of thermodynamic properties as an expansion from the zero-density limit. The virial expansion is given by

$$\frac{p}{\rho RT} = 1 + B(T)\rho + C(T)\rho^2 + \dots, \quad (1)$$

where p is the pressure, ρ is the molar density, R is the molar gas constant, and T is the thermodynamic temperature. The second virial coefficient $B(T)$ depends only on the interaction between a pair of molecules, $C(T)$ depends on interactions among three molecules, etc.

A similar expansion for the square of the speed of sound w introduces a second acoustic virial coefficient $\beta_a(T)$, third acoustic virial coefficient $\gamma_a(T)$, etc.:

$$w^2 = \frac{\gamma_0 RT}{M} \left[1 + \beta_a(T) \frac{p}{RT} + \gamma_a(T) \frac{p^2}{RT} + \dots \right], \quad (2)$$

where γ_0 is the ratio of the isobaric to the isochoric heat capacity in the ideal-gas limit (exactly 5/3 for a monatomic species) and M is the molar mass. The acoustic virial coefficients are functions of B and C and their first two temperature derivatives. For example, the second acoustic virial coefficient is

$$\beta_a(T) = 2B(T) + 2(\gamma_0 - 1)T \frac{dB(T)}{dT} + \frac{(\gamma_0 - 1)^2}{\gamma_0} T^2 \frac{d^2B(T)}{dT^2}. \quad (3)$$

In the past 30 years, improvements in computational quantum mechanics have allowed the pair potential between two helium atoms to be calculated with extraordinary accuracy. Since fully quantum-mechanical computations of $B(T)$ and $\beta_a(T)$ from the pair potential can be performed with an exact phase-shift method, these coefficients can be obtained rigorously with very small uncertainties. For the state-of-the-art helium pair potential published in 2020 [14], the relative uncertainty in computed values of B near room temperature is on the order of 10^{-5} .

However, it may not be appreciated that it is not easy to maintain these tiny uncertainties for temperatures other than those at which the virial coefficients are tabulated. Added uncertainty due to interpolation between the tabulated points can be larger than the uncertainty of the calculated values. This is analogous to the “nonuniqueness” uncertainty that arises in thermometry, where the small uncertainties at fixed calibration points increase for temperatures between the fixed points due to the use of different interpolation functions and/or different thermometers that do not behave identically [15].

In this paper, we will show (using the state-of-the-art results for $B(T)$ and $\beta_a(T)$) that these interpolation errors can be significant. After finding that no interpolation method based on the tables for helium in Ref. [14] is fully adequate, we offer a different approach that allows $B(T)$ and $\beta_a(T)$ to be computed at any temperature of interest for metrology without loss of accuracy.

The two other noble gases used in metrology are neon and argon. The greater number of electrons on these atoms results in pair potentials that do not achieve the tiny uncertainties attained for helium, but they are still accurate enough to be useful. The state-of-the-art potential for neon [16] produces second virial coefficients whose uncertainty is similar to that of most of the best experimental data (although it is inferior to a very accurate experimental result [17] at 273.16 K). The state of the art for argon [18] does not quite match the uncertainties of the best experimental data (see Fig. 7 in Ref. [18]). Calculated virial coefficients for neon and argon are, however, needed for metrology outside the temperature range of the low-uncertainty experimental data. We apply our new approach to these gases as well.

2. Interpolation for $B(T)$ and $\beta_a(T)$

We begin with $B(T)$ and $\beta_a(T)$ for helium, because those quantities can be calculated with extremely small uncertainties, making small errors from interpolation more significant on a relative basis. These coefficients can be calculated exactly with a phase-shift method, as described by Hurly and Mehl [19] among others. The implementation of this calculation is challenging, but once the phase shifts are found for a given pair potential they can be used to compute the virial coefficients at any temperature (limited at the high-temperature end only by the number of phase shifts calculated, since the number needed for convergence increases with temperature) with relatively little additional effort. This allows us to obtain results at other temperatures with uncertainties as small as those tabulated in Ref. [14].

Czachorowski *et al.* [14] tabulated (as Supplemental Material) $B(T)$ and $\beta_a(T)$ and their uncertainties for both ^4He and ^3He at 122 temperatures ranging from 0.5 K to 1000 K. While they did not assign a statistical meaning to their uncertainties, metrologists typically treat them as expanded uncertainties with coverage factor $k = 2$, roughly corresponding to a 95 % confidence interval. No guidance was given for interpolating between the tabulated points.

The simplest physically reasonable interpolations one might consider are linear interpolation in T and linear interpolation in $1/T$. One could also consider interpolation that makes use of additional points in the table, the most familiar of which is the cubic spline.

In Fig. 1, we show different interpolation schemes for $B(T)$ of ^4He between the tabulated points at 5 K and 5.5 K. The baseline is linear interpolation in T , and curves are plotted representing interpolation linear in $1/T$ and cubic spline interpolation. We also plot the correct value at 5.25 K that we calculated with the phase-shift method,

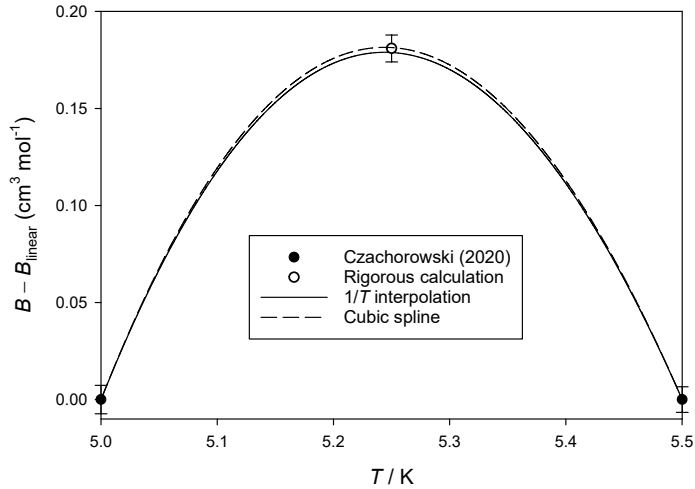


Figure 1. Comparison of interpolation to rigorous calculation for $B(T)$ of ${}^4\text{He}$ at 5.25 K. The baseline for the plot is linear interpolation in T . Error bars represent expanded ($k = 2$) uncertainties.

with error bars corresponding to its expanded uncertainty. The interpolation approach clearly matters; the discrepancies among different interpolation methods are many times larger than the expanded uncertainty of the $B(T)$ points. At this temperature, both the cubic spline and the simpler $1/T$ interpolation perform well.

Since cubic spline interpolation is not trivial (for example, it is not a native function in common spreadsheet software), one might hope that $1/T$ interpolation would be adequate everywhere. Alas, this is not the case. In Fig. 2, we show a similar plot between 500 K and 550 K, with a rigorously calculated value at the midpoint of 525 K. This time $1/T$ interpolation is worse than linear interpolation, and both of them are in error by more than 10 times the expanded uncertainty of the calculation. Only the cubic spline interpolation is acceptable in this case.

Rather than examining one temperature at a time, we can perform this comparison for all 121 temperature midpoints from Ref. [14], allowing us to assess different interpolations throughout the temperature range. For this, we define the interpolation error in the second virial coefficient B :

$$\Delta B = B_{\text{interp}} - B_{\text{rig}}, \quad (4)$$

where B_{interp} is the value obtained by interpolation and B_{rig} is that obtained from the rigorous phase-shift calculation. We define an analogous quantity for the second acoustic virial coefficient β_a :

$$\Delta\beta_a = \beta_{a,\text{interp}} - \beta_{a,\text{rig}}. \quad (5)$$

We then normalize ΔB and $\Delta\beta_a$ by the expanded uncertainties of the rigorously computed values, $U(B)$ and $U(\beta_a)$. Ideally, we want the magnitude of this ratio to

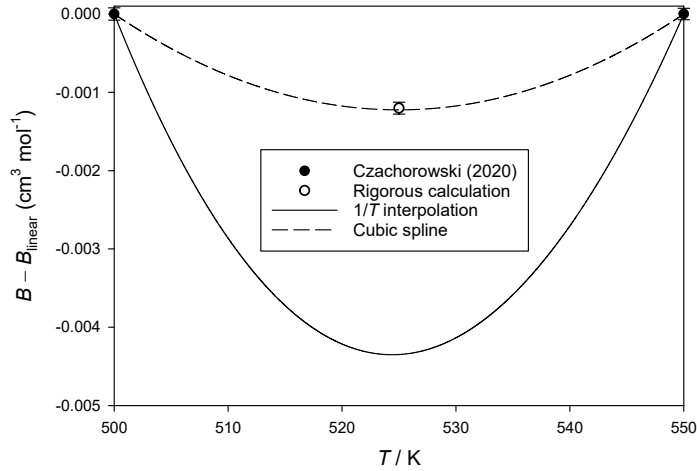


Figure 2. Comparison of interpolation to rigorous calculation for $B(T)$ of ${}^4\text{He}$ at 525 K. The baseline for the plot is linear interpolation in T . Error bars represent expanded ($k = 2$) uncertainties.

be less than approximately 0.3 so that interpolation errors do not add significantly to the overall uncertainty.

Figure 3 shows the results of this exercise for $B(T)$ of ${}^4\text{He}$ with both linear and $1/T$ interpolation. Each point represents one temperature at the midpoint of adjacent tabulated values. In this figure and also in Figs. 4–6, the basis for interpolation is values of B computed in this work. As discussed in Sec. 5.1, these differ slightly at higher temperatures from the results tabulated in Ref. [14], and we do not want that difference to distort our analysis.

It is clear from Fig. 3 that neither interpolation method is suitable for the table in Ref. [14]. $1/T$ interpolation is accurate between about 4 K and 40 K, but not at lower or higher temperatures, and linear interpolation is poor at almost all temperatures.

We display the same information for cubic spline interpolation on a figure with a different vertical scale. Figure 4 shows that the cubic spline, while generally much better than linear or $1/T$ interpolation, produces an error that is larger than desired at the very lowest temperatures and above roughly 500 K.

An alternative “interpolation” method that is convenient in practice is to use an empirical fitting equation. For purposes of differentiation for computing acoustic virial coefficients, Binosi et al. [20] developed an equation for $B(T)$ of helium that passed through the tabulated points of Czachorowski et al. [14] between 2 K and 1000 K within their expanded uncertainties $U(B)$. [Unfortunately, some exponents were improperly truncated in Ref. [20]; corrected values for the $B({}^4\text{He})$ fit in Table III of that paper are $b_3 = 0.801\,564\,7$, $b_4 = 0.301\,417\,8$, $b_5 = 0.260\,487\,5$, $b_6 = 0.225\,976\,1$.] The solid curve in Fig. 4 shows the error of the (corrected) smoothing equation of Binosi et al.; at most temperatures it introduces more error than cubic spline interpolation. While the

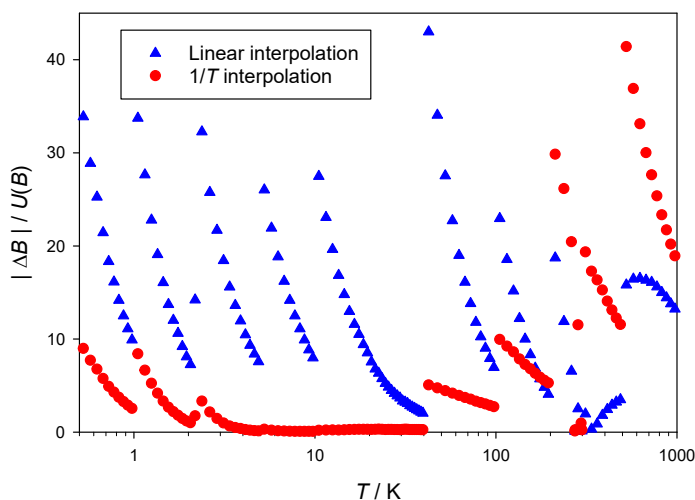


Figure 3. Magnitude of error of linear and $1/T$ interpolations for $B(T)$ of ${}^4\text{He}$, normalized by expanded uncertainty in B .

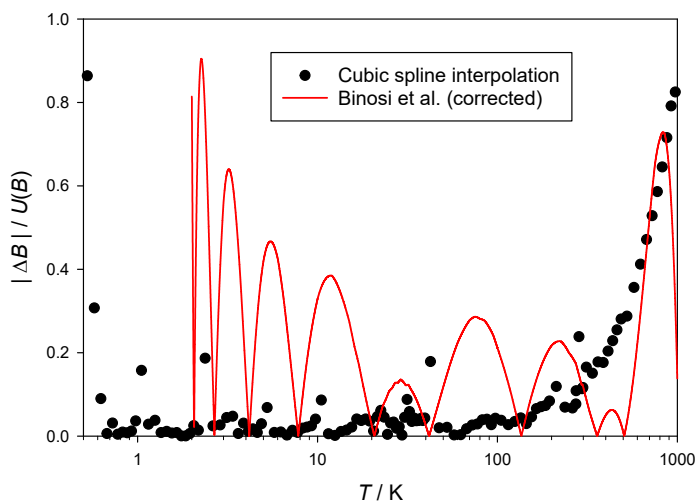


Figure 4. Magnitude of error of cubic spline interpolation for $B(T)$ of ${}^4\text{He}$, along with that of the corrected smoothing equation of Binosi et al. [20] that was fitted for $2 \leq T/K \leq 1000$, normalized by expanded uncertainty in B .

smoothing equation could have been improved somewhat by adding additional terms, it would be quite difficult to produce an equation that even approached the accuracy of the cubic spline. The lesson from examination of this equation is that, for highly accurate calculated data, a fitted equation does not eliminate the errors arising from interpolation, and will likely be worse than spline interpolation.

The situation for linear, $1/T$, and cubic spline interpolation is similar for β_a ; the

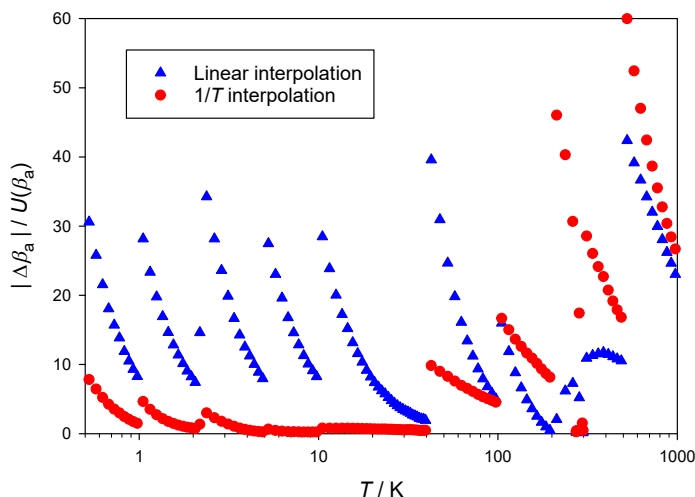


Figure 5. Magnitude of error of linear and $1/T$ interpolation for $\beta_a(T)$ of ${}^4\text{He}$, normalized by expanded uncertainty in β_a .

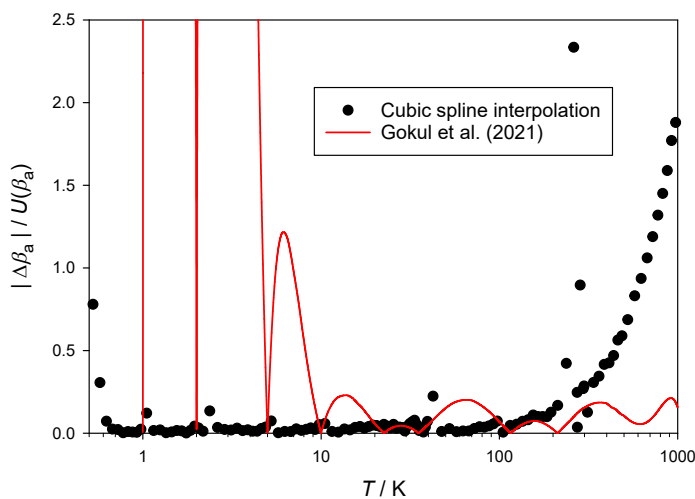


Figure 6. Magnitude of error of cubic spline interpolation for $\beta_a(T)$ of ${}^4\text{He}$, along with that of the smoothing equation of Gokul et al. [21] that was fitted for $1 \leq T/\text{K} \leq 1000$, normalized by expanded uncertainty in β_a .

ratios shown in Figs. 5 and 6 are similar in magnitude to those in Figs. 3 and 4 for $B(T)$. The range of temperatures where errors of cubic spline interpolation are undesirably large extends to below 300 K. A point in Fig. 6 near 262 K is an outlier; this results from poor spacing in a spline that uses tabulated points at 273.15 K and 273.16 K. Other points lying above the general trend are also a consequence of splines through unevenly spaced tabulated points; distortion when the spacing of the points is very uneven is an underappreciated danger when using spline interpolation.

Figure 6 also provides another illustration of an empirical smoothing equation. Gokul et al. [21] provided a 10-term equation fitted to the values of β_a tabulated by Czachorowski et al. [14]. The solid curve in Fig. 6 shows the normalized error of their equation as a function of temperature. Its performance is adequate above 10 K (better than the cubic spline above 200 K), but not at lower temperatures, especially below 5 K where the error metric is mostly off the scale of the plot, exceeding 100 at some temperatures below 2 K.

We conclude that no straightforward interpolation approach can be consistently trusted to provide $B(T)$ and $\beta_a(T)$ without the possibility of introducing significant additional uncertainty.

Similar analysis can be performed for neon and argon, based on literature tabulations from state-of-the-art potentials [16, 18]. Since the relative uncertainties of these pair potentials (and therefore of the calculated B and β_a) are somewhat larger, the requirements for interpolation are not as severe, and cubic spline interpolation might be expected to be adequate. Unfortunately, that turns out to not always be the case.

In Fig. 7, we show the interpolation errors for cubic spline interpolation based on the $B(T)$ tables published by Hellmann et al. [16] for neon (calculated for natural neon as described below) and of Lang et al. [18] for argon. For the majority of temperatures for both substances, the interpolation error is indeed negligible. For neon, the interpolation error becomes large below 10 K; this appears to be due to the large spacing (in relative terms) of tabulated temperatures in this region (such low temperatures are unlikely to be of practical importance for metrology using neon). Four points near 273 K also have larger errors; this is caused by splines with uneven spacing due to tabulated points at 273.15 K and 273.16 K. For argon, there are many points with significant interpolation errors, with the normalized error reaching a maximum near 16.5 at 316.7395 K. This is caused by a number of cases where the table contains points that are only 0.01 K or even 0.001 K apart in temperature.

We conclude that the existing state-of-the-art tabulated $B(T)$ for neon and argon cannot be reliably used with cubic spline interpolation without the possibility of introducing interpolation errors that are significant compared to the uncertainty of the calculated $B(T)$. Most of these errors can be reduced by manually deleting one of each pair of closely spaced points in the tables before applying cubic splines, but that is an awkward solution. In the following, we describe an approach that allows users of these state-of-the-art virial-coefficient calculations to avoid interpolation altogether.

3. Avoiding Interpolation with Precalculated Phase Shifts

One of us initially had the idea of a brute-force approach to minimize the aforementioned interpolation errors by generating a more finely spaced table. A criterion for the spacing could be that simple linear interpolation (or perhaps cubic spline interpolation) give a ratio $|\Delta B|/U(B)$ less than 0.3 at all temperatures. This would require thousands or millions of temperatures in each table.

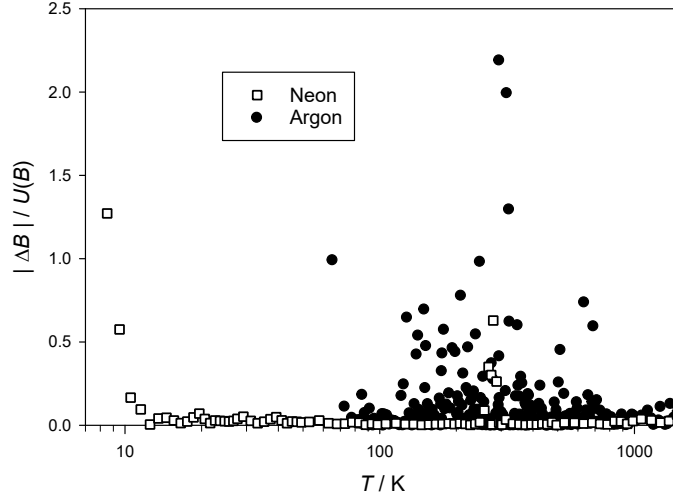


Figure 7. Magnitude of error of cubic spline interpolation for $B(T)$ of neon and argon, based on the potentials of Hellmann et al. [16] for Ne (calculations performed for natural neon) and Lang et al. [18] for Ar. Three points for neon at 5.5 K, 6.5 K, and 7.5 K and two points for argon at 316.7395 K and 319.075 K are above the vertical scale of the figure.

It was realized that a more elegant approach is to avoid interpolation completely by calculating and publishing data structures containing the quantum-mechanical phase shifts and bound-state energies for each pair potential. This information takes several megabytes for each pair, but that is not a problem for modern computers. Simple scripts can then be provided to calculate $B(T)$ and $\beta_a(T)$ at any temperature desired. In the following sections, we will describe the calculation of phase shifts and their use in calculation of low-density thermodynamic properties.

4. Thermophysical Properties at the Two-Body Level

The second virial coefficient of a monatomic gas is given by [22, 23, 24]

$$B(T) = B_{\text{th}}(T) + B_{\text{bound}}(T) + B_{\text{xc}}(T), \quad (6)$$

where

$$B_{\text{th}}(T) = -N_A \Lambda_\mu^3 \sum_{l=0}^{\infty} (2l+1) \left(1 + \frac{(-1)^{l+2I}}{2I+1} \right) \times \int_0^{\infty} e^{-\Lambda_\mu^2 k^2 / (4\pi)} \delta_l(k) \left(\frac{\Lambda_\mu}{2\pi} \right)^2 k \, dk \quad (7)$$

$$B_{\text{bound}}(T) = -\frac{N_A \Lambda_\mu^3}{2} \sum_{l=0}^{\infty} (2l+1) \left(1 + \frac{(-1)^{l+2I}}{2I+1} \right) \sum_{n=0}^{N_l} (e^{-\beta E_{n,l}} - 1) \quad (8)$$

$$B_{\text{xc}}(T) = -\frac{N_A \Lambda_\mu^3}{16} \frac{(-1)^{2I}}{2I+1}, \quad (9)$$

where—with N_A the Avogadro constant, k_B the Boltzmann constant, $\hbar = h/(2\pi)$ the reduced Planck constant, and μ the reduced mass of the particles—we have defined $\beta = (k_B T)^{-1}$ and $\Lambda_\mu = h\sqrt{\beta/(2\pi\mu)}$. In Eq. (7), $\delta_l(k)$ is the *absolute* phase shift for scattering at energy $E = \hbar^2 k^2/(2\mu)$ and relative angular momentum $\hbar l$, while in Eq. (8) the quantity $E_{n,l}$ is the energy of the n -th bound state when the particles are in a state with relative angular momentum $\hbar l$. In Eqs. (7)–(9), I denotes the nuclear spin of the gas particles. These equations are also valid for calculation of the cross virial coefficient for non-identical particles (*e.g.*, ^4He with ^3He), provided that in this case one takes the limit $I \rightarrow \infty$. Note that in the case of spinless particles ($I = 0$), only even values of l contribute to the sums in Eqs. (7) and (8).

The second acoustic virial coefficient of a monatomic gas is given by Eq. (3) and requires $B(T)$ and its first two temperature derivatives. The evaluation of the temperature derivatives of $B(T)$ from Eqs. (7)–(9) is straightforward, recalling the definition of β and that

$$\frac{d\Lambda_\mu}{dT} = -\frac{\Lambda_\mu}{2T}. \quad (10)$$

It is convenient to define

$$S(k) = \sum_{l=0}^{\infty} (2l+1) \left(1 + \frac{(-1)^{l+2I}}{2I+1}\right) \delta_l(k) \quad (11)$$

$$I_n(T) = -N_A \frac{\Lambda_\mu^5}{4\pi^2} \int e^{-\Lambda_\mu^2 k^2/(4\pi)} S(k) k^{n+1} dk, \quad (12)$$

so that $B_{\text{th}}(T) = I_0(T)$. Performing the temperature derivatives, one finds:

$$T \frac{dB_{\text{th}}}{dT} = -\frac{5}{2} I_0(T) + \frac{\Lambda_\mu^2}{4\pi} I_2(T) \quad (13)$$

$$T \frac{dB_{\text{bound}}}{dT} = -\frac{N_A \Lambda_\mu^3}{2} \sum_{l=0}^{\infty} (2l+1) \left(1 + \frac{(-1)^{l+2I}}{2I+1}\right) \times \sum_{n=0}^{N_l} \left[-\frac{3}{2} (e^{-\beta E_{n,l}} - 1) + \beta E_{n,l} e^{-\beta E_{n,l}} \right] \quad (14)$$

$$T \frac{dB_{\text{xc}}}{dT} = -\frac{3}{2} B_{\text{xc}}(T), \quad (15)$$

and

$$T^2 \frac{d^2 B_{\text{th}}}{dT^2} = \frac{35}{4} I_0(T) - 7 \frac{\Lambda_\mu^2}{4\pi} I_2(T) + \left(\frac{\Lambda_\mu^2}{4\pi}\right)^2 I_4(T) \quad (16)$$

$$T^2 \frac{d^2 B_{\text{bound}}}{dT^2} = -\frac{N_A \Lambda_\mu^3}{2} \sum_{l=0}^{\infty} (2l+1) \left(1 + \frac{(-1)^{l+2I}}{2I+1}\right) \times \sum_{n=0}^{N_l} \left[\frac{15}{4} (e^{-\beta E_{n,l}} - 1) + \beta E_{n,l} (\beta E_{n,l} - 5) e^{-\beta E_{n,l}} \right] \quad (17)$$

$$T^2 \frac{d^2 B_{\text{xc}}}{dT^2} = \frac{15}{4} B_{\text{xc}}(T). \quad (18)$$

5. Calculation of Phase Shifts and Bound States

We computed the absolute phase shifts by solving the radial Schrödinger equation using the renormalized Numerov approach [25] and following the procedure described in Ref. [26].

5.1. Helium-3 and helium-4

In the case of helium isotopes, we used the latest pair potentials by Czachorowski *et al.* [14], which incorporate corrections beyond the nonrelativistic Born–Oppenheimer approximation—including adiabatic, nonadiabatic, relativistic, and quantum electrodynamic effects—that lead to slight isotopic differences in the pair potential. The phase shifts were computed for N_E logarithmically spaced energies ranging from 10^{-5} K to 1 hartree ($\approx 315\,775$ K); we used $N_E = 1536$ for ^4He and $N_E = 1024$ for ^3He and for the cross value. We integrated the radial Schrödinger equation for angular momenta up to $L = 1600$ for ^4He and $L = 1000$ for ^3He and the ^3He – ^4He system, using the same integration step suggested by Hurly and Mehl [19].

These choices were enough to obtain converged values that matched the published values of $B(T)$ within their quoted uncertainty [14] up to a temperature $T_{\text{max}} = 1500$ K, as shown in Fig. 8. We notice a slight systematic deviation between our computed values of $B(T)$ and those reported in the original paper [14]; in particular, our values are lower. We checked the convergence as a function of the angular momentum states used in the calculation, and verified that the limiting value is approached *from above*. Therefore, our findings suggest a slightly incomplete convergence with respect to the number of angular momentum states in the values reported in Ref. [14]. Nevertheless, we note that the difference in this case is roughly 1/3 the magnitude of the expanded uncertainty propagated from the imperfect knowledge of the potential, so that our results and those in the original publication are consistent. A comparison of our calculated β_a to those from Ref. [14] is very similar to that for B in Fig. 8.

When solving for the bound states, we diagonalized the pair Hamiltonian using LAPACK’s `dsteibz` routine [27]. The bound halo state of the ^4He dimer [14] was resolved by using a radial cutoff of $R = 50$ nm and a discretization step of $h = 10^{-4}$ nm.

5.2. Neon

In the case of neon, we used the pair potential by Hellmann *et al.* [16]. In this case, we used 1024 logarithmically spaced values for the collision energy in the same energy range as for helium. Phase shifts were computed up to $L = 1200$, and bound states were computed using a radial cutoff of $R = 10$ nm with the same discretization step as for helium.

Neon has three stable isotopes: ^{20}Ne , ^{21}Ne , and ^{22}Ne ; we computed phase shifts and bound states for all six pairwise combinations of these. The resulting values of B_{ij} for

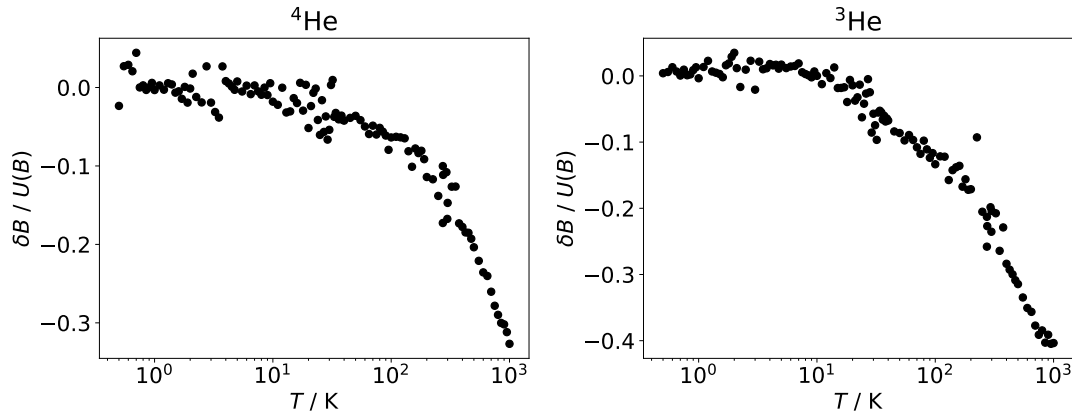


Figure 8. The ratio $\delta B/U(B)$ for ^4He (left panel) and ^3He (right panel). δB is the difference between the values of $B(T)$ computed in this work and those reported in [14], while $U(B)$ is the $k = 2$ uncertainty of $B(T)$ computed by propagating the uncertainty of the pair potential [14].

each pair can be used to compute $B(T)$ for neon of any isotopic composition according to

$$B = \sum_{i,j} x_i x_j B_{ij}, \quad (19)$$

where x_i is the fraction of isotope i .

For naturally occurring neon, the nominal composition [28] is 0.9048, 0.0027, and 0.0925 for isotopes 20, 21, and 22, respectively. Calculations of $B(T)$ for this composition agree with the published ones [16] within mutual uncertainty up to a temperature of 1500 K, as shown in the left panel of Fig. 9.

5.3. Argon

In the case of argon, we used the pair potential by Lang *et al.* [18]. We considered the same collision energies as for neon, but we computed phase shifts up to $L = 2000$. Bound states were computed using the same procedure as for neon. Also in this case, we verified that the values of the second virial coefficient agree with the published results in the temperature range $10 \leq T \leq 1500$ K, as reported in the right panel of Fig. 9. The arrow-like shape of this plot is unusual; we could not identify its origin but it may reflect some calculational detail in Ref. [18]. This feature does not affect the agreement between our calculations and those of Ref. [18], which remains within approximately 10 % of the expanded uncertainty.

The argon results are computed for the ^{40}Ar isotope. Because this isotope is 99.6 % of natural argon, and because mass-dependent quantum effects are smaller for argon than for Ne and (especially) He, the error introduced by this simplification is negligible compared to the effect of the uncertainty of the pair potential.

The agreement with published β_a for both neon and argon is similar to that shown for B in Fig. 9.

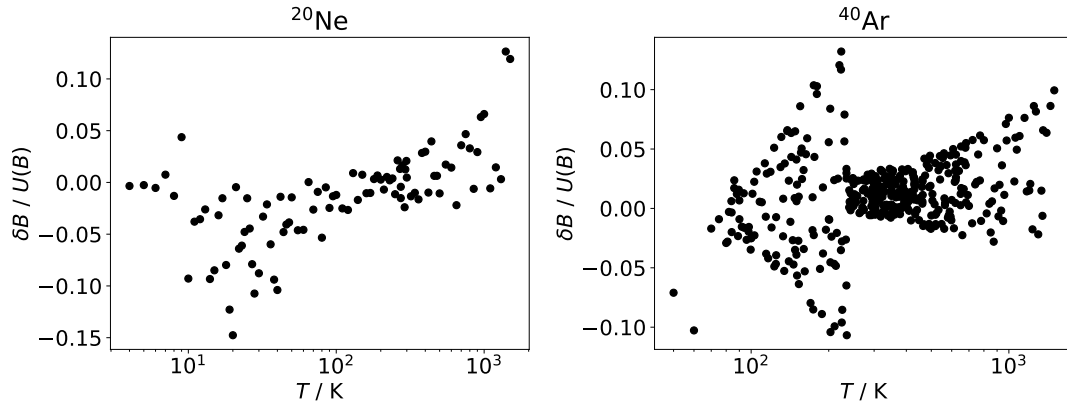


Figure 9. The ratio $\delta B/U(B)$ for ^{20}Ne (left panel) and ^{40}Ar (right panel). δB is the difference between the values of $B(T)$ computed in this work and those reported in [16] for ^{20}Ne and [18] for ^{40}Ar . $U(B)$ is the $k = 2$ uncertainty of $B(T)$ computed by propagating the uncertainty of the pair potential [16, 18].

5.4. Format of the data file

All the phase shifts and bound-state energies required to perform the computation have been collected into compressed JSON [29] files and are available, together with a Python [30, 31, 32] program to compute the second virial coefficient, its first two temperature derivatives, and the second acoustic virial coefficient, at the web address <https://www.github.com/gioGarbe/TAPPS>. The relevant files are also available in the NIST Public Data Repository [33]. Once uncompressed, the JSON files present all the information organized hierarchically in text format: some metadata describe the content of the file and reference the pair potential used. These are followed by the minimum and maximum temperature for which we expect the calculation to be reliable, data about the system being computed (reduced mass and nuclear spin), followed by a list of bound states, the angular momenta and relative energies for which the phase shifts have been computed, and the phase shifts themselves.

It is intended that the JSON files can be replaced with updated versions if and when an improved pair potential is developed for any of these three gases; the Python programs would not need to be modified.

6. Discussion and Conclusions

We showed in Sec. 2 that, with the existing state of the art for second density and acoustic virial coefficients for helium, neon, and argon, interpolation of published tables can lead to errors that are significant compared to the uncertainty of the tabulated values. Cubic spline interpolation is often adequate if the points are not too far apart, but it can produce unexpectedly large errors if the spacing of temperatures in the table is uneven. By providing simple Python scripts along with data structures containing phase shifts calculated from state-of-the-art potentials, we have provided the ability for

researchers to calculate these quantities at any temperature of metrological interest, completely avoiding interpolation.

The phase shifts provided in conjunction with this paper are sufficient to calculate $B(T)$ up to 1500 K with relative uncertainty due to omitted phase shifts less than 10^{-6} for ^4He , 5×10^{-5} for Ne isotopes, and 10^{-4} for ^{40}Ar . This upper temperature limit is chosen because of efforts in progress to apply acoustic gas thermometry up to the copper point, which is approximately 1358 K [2, 34]. Reaching higher calculated temperatures is straightforward, but would require computing phase shifts for higher angular momenta, resulting in substantially larger data files.

At very low temperatures, the bound-state contribution to $B(T)$ diverges as $-\exp(1/T)$. This requires setting a lower temperature limit in the software, which we have chosen as 0.01 K for ^3He and ^4He , 1 K for Ne, and 10 K for Ar. These temperatures are below the ranges relevant to any gas-based metrology that we can envision.

We have produced data structures containing accurately calculated phase shifts for ^3He , ^4He , Ne, and Ar, including the ^3He – ^4He interaction and the isotopic combinations required to rigorously describe neon. Simple Python scripts then allow the calculation of B and β_a at any temperature up to 1500 K (and above 0.01 K for He, 1 K for Ne, and 10 K for Ar). The data files and scripts for these calculations are freely available at <https://www.github.com/gioGarbe/TAPPS> and in the NIST Public Data Repository [33]. These calculations can be used directly in data analysis for thermodynamic metrology, eliminating uncertainty due to interpolation. In some cases, software that runs experiments may require faster calculations than can be achieved by this method; in those cases, our approach can be used to generate in advance a fine grid of points in the temperature range of interest that can be used for interpolation within the software.

In principle, uncertainties in $B(T)$ and $\beta_a(T)$ could be computed similarly by computing upper and lower values from additional tables of phase shifts precalculated for positively and negatively perturbed potentials corresponding to the uncertainty of the potential. However, because there is substantial subjective judgment involved in estimating the uncertainties of the pair potentials, the uncertainties in the second virial quantities are themselves rather uncertain. Therefore, nothing meaningful is lost by simply linearly interpolating the tabulated uncertainties.

A natural extension of this work would be the computation of transport properties (e.g., viscosity, thermal conductivity). No additional potential-specific data apart from the phase shifts is required, but additional scripts of moderate complexity would be necessary to implement the calculation of the generalized cross sections and higher-order correction factors needed to compute the transport properties [19, 35].

Acknowledgments

A.H. acknowledges helpful discussions with Patrick Egan, Mike Moldover, and Patrick Rourke.

- [1] M R Moldover, R M Gavioso, J B Mehl, L Pitre, M de Podesta, and J T Zhang. Acoustic gas thermometry. *Metrologia*, 51:R1–R19, 2014.
- [2] L Xing, X-J Feng, M-H Si, J-T Zhang, H Lin, K A Gillis, and M R Moldover. Cylindrical acoustic gas thermometry. *J. Phys. Chem. Ref. Data*, 52:031501, 2023.
- [3] C Gaiser, T Zandt, and B Fellmuth. Dielectric-constant gas thermometry. *Metrologia*, 52:S217–S226, 2015.
- [4] C Gaiser, B Fellmuth, and W Sabuga. Primary gas-pressure standard from electrical measurements and thermophysical ab initio calculations. *Nature Phys.*, 16:177–180, 2020.
- [5] C Gaiser, B Fellmuth, and W Sabuga. Primary gas pressure standard passes next stress test. *Ann. Physik*, 534:2200336, 2022.
- [6] P M C Rourke, C Gaiser, B Gao, D Madonna Ripa, M R Moldover, L Pitre, and R J Underwood. Refractive-index gas thermometry. *Metrologia*, 56:032001, 2019.
- [7] P M C Rourke. Perspective on the refractive-index gas metrology data landscape. *J. Phys. Chem. Ref. Data*, 50:033104, 2021.
- [8] P F Egan, J A Stone, J E Ricker, J H Hendricks, and G F Strouse. Cell-based refractometer for pascal realization. *Opt. Lett.*, 42:2944–2947, 2017.
- [9] P F Egan and Y Yang. Optical $n(p, T_{90})$ measurement suite 1: He, Ar, and N₂. *Int. J. Thermophys.*, 44:181, 2023.
- [10] P Gambette, R M Gavioso, D Madonna Ripa, M D Plimmer, F Sparasci, and L Pitre. Toward the realization of a primary low-pressure standard using a superconducting microwave resonator. *Rev. Sci. Instrum.*, 94:035112, 2023.
- [11] I Silander, J Zakrisson, O Axner, and M Zelan. Realization of the pascal based on argon using a Fabry–Perot refractometer. *Opt. Lett.*, 49:3296–3299, 2024.
- [12] Y Yang, J A Stone, and P F Egan. Demonstration of dispersion gas barometry. *Phys. Rev. Applied*, 23:064041, 2025.
- [13] G Garberoglio, C Gaiser, R M Gavioso, A H Harvey, R Hellmann, B Jeziorski, K Meier, M R Moldover, L Pitre, K Szalewicz, and R Underwood. Ab initio calculation of fluid properties for precision metrology. *J. Phys. Chem. Ref. Data*, 52:031502, 2023.
- [14] P Czachorowski, M Przybytek, M Lesiuk, M Puchalski, and B Jeziorski. Second virial coefficients for ⁴He and ³He from an accurate relativistic interaction potential. *Phys. Rev. A*, 102:042810, 2020.
- [15] B W Mangum, P Bloembergen, M V Chattle, B Fellmuth, P Marcarino, and A I Pokhodun. On the International Temperature Scale of 1990 (ITS-90). Part I: Some definitions. *Metrologia*, 34:427–429, 1997.
- [16] R Hellmann, C Gaiser, B Fellmuth, T Vasytsova, and E Bich. Thermophysical properties of low-density neon gas from highly accurate first-principles calculations and dielectric-constant gas thermometry measurements. *J. Chem. Phys.*, 154:164304, 2021.
- [17] C Gaiser and B Fellmuth. Highly-accurate density-virial-coefficient values for helium, neon, and argon at 0.01 °C determined by dielectric-constant gas thermometry. *J. Chem. Phys.*, 150:134303, 2019.
- [18] J Lang, M Przybytek, and M Lesiuk. Thermophysical properties of argon gas from improved two-body interaction potential. *Phys. Rev. A*, 109:052803, 2024.
- [19] J J Hurly and J B Mehl. ⁴He thermophysical properties: New ab initio calculations. *J. Res. Nat. Inst. Stand. Technol.*, 112:75–94, 2007.
- [20] D Binosi, G Garberoglio, and A H Harvey. The third density and acoustic virial coefficients of helium isotopologues from *ab initio* calculations. *J. Chem. Phys.*, 160:244305, 2024.
- [21] N Gokul, A J Schultz, and D A Kofke. Speed of sound in helium-4 from ab initio acoustic virial coefficients. *J. Chem. Eng. Data*, 66:3258–3281, 2021.
- [22] J De Boer and A Michels. Quantum-mechanical calculation of the second virial-coefficient of helium at low temperatures. *Physica*, 6:409–420, 1939.

- [23] J E Kilpatrick, W E Keller, E F Hammel, and N Metropolis. Second virial coefficients of He³ and He⁴. *Phys. Rev.*, 94:1103–1110, 1954.
- [24] M E Boyd, S Y Larsen, and J E Kilpatrick. Quantum mechanical second virial coefficient of a Lennard-Jones gas. Helium. *J. Chem. Phys.*, 50:4034–4055, 1969.
- [25] B R Johnson. New numerical methods applied to solving the one-dimensional eigenvalue problem. *J. Chem. Phys.*, 67:4086–4093, 1977.
- [26] H Wei and R J Le Roy. Calculation of absolute scattering phase shifts. *Mol. Phys.*, 104:147–150, 2006.
- [27] E Anderson, Z Bai, C Bischof, S Blackford, J Demmel, J Dongarra, J Du Croz, A Greenbaum, S Hammarling, A McKenney, and D Sorensen. *LAPACK Users' Guide*. Society for Industrial and Applied Mathematics, Philadelphia, PA, third edition, 1999.
- [28] J Meija, T B Coplen, M Berglund, W A Brand, P De Bièvre, M Gröning, N E Holden, J Irrgeher, R D Loss, T Walczyk, and T Prohaska. Atomic weights of the elements 2013 (IUPAC Technical Report). *Pure Appl. Chem.*, 88:265–291, 2016.
- [29] International Organization for Standardization. Information technology – The JSON data interchange syntax. ISO/IEC 21778:2017, 2017. <https://www.iso.org/standard/71616.html>.
- [30] Python Software Foundation. Python language reference, version 3.10, 2025.
- [31] C R Harris, K J Millman, S J van der Walt, et al. Array programming with NumPy. *Nature*, 585:357–362, 2020.
- [32] P Virtanen, R Gommers, T E Oliphant, et al. SciPy 1.0: Fundamental algorithms for scientific computing in Python. *Nature Methods*, 17:261–272, 2020.
- [33] G Garberoglio and A H Harvey. Phase-shift data for fully quantum calculations of thermophysical properties for noble gases. National Institute of Standards and Technology, 2025. <https://doi.org/10.18434/mds2-3802>.
- [34] X Feng, K A Gillis, M R Moldover, and J B Mehl. Microwave-cavity measurements for gas thermometry up to the copper point. *Metrologia*, 50:219–226, 2013.
- [35] J O Hirschfelder, C F Curtiss, and R B Bird. *Molecular Theory of Gases and Liquids*. John Wiley & Sons, New York, 1954.